Hardware Requirement of Active Reconfigurable Intelligent Surface for A Single-User Single-Input Single-Output Non-Line-of-Sight 5G Communication System

Apisak Worapishet

Mahanakorn Institute of Innovation, Mahanakorn University of Technology
140 Cheumsamphan Road, Kratumrai, Nongchok, Bangkok, Thailand 10530
Email: apisakw@mut.ac.th

Manuscript Received November 23, 2024
Revised December 8, 2024
Accepted December 16, 2024

ABSTRACT

A hardware specification of an active reconfigurable intelligent surface (aRIS), which possesses the capability to mitigate the adverse multiplicative fading effect in non-line-of-sight communication systems employing a reflective antenna, is investigated. By utilizing the link budget analysis approach, the salient characteristic and operational insight of an aRIS are outlined and discussed. For a specific example of an aRIS-assisted single-user single-input single-output wireless communication system operating at millimeter-wave frequencies, For a specific example of an aRIS-assisted single-user single-input single-output wireless communication system operating at millimeter-wave frequencies, the required gain, power, linearity, and noise figure of the aRIS's active circuit are determined under both normal and weak path loss conditions. Discussion on performance trade-off is also given.

Keywords: *Reconfigurable Intelligent Surface (RIS), active RIS, active reflector, NLOS, 5G system*

1. INTRODUCTION

Nowadays, the reconfigurable intelligent surface (RIS) has been recognized as a feasible, inexpensive and low power means to improve channel capacity and expand area coverage of state-of-the-art wireless communications, including millimeter-wave 5G network, as well as future 6G networks and beyond [1] – [6]. This fact has been exemplified by a plethora of research papers on the RIS over the last few years, covering both the hardware implementation [7] – [10], and mostly the analysis of the communication performance [3] – [6]. The RIS can be categorized into passive and active RIS types [6]. Recent research works, however, have focused mainly on the active RIS or *a*RIS, because of its ability to mitigate the adverse multiplicative fading effect associated with any type of reflective antennas through an introduction of amplification into the reflected signal [6 – 7], [10].

While majority of published works have focused on the channel characterization and optimization of *a*RIS-assisted communication system performance, most of the *a*RIS hardware implementation only demonstrated circuit techniques without considering the required performance for any specific communication system scenario [7] – [10].

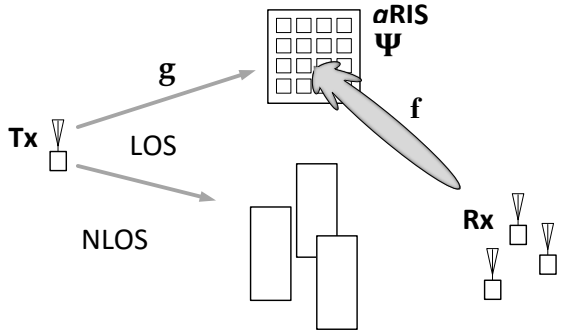

Fig. 1 *Typical aRIS-assisted NLOS wireless communication system.*

To address the lack of hardware specification requirement for an *a*RIS implementation in the existing literature, it is the purpose of this paper to determine, by virtue of the link budget analysis, the electrical specification of an *a*RIS's *active circuit*, in terms of gain, noise figure, output power, and linearity, for given specifications of transmitter (Tx), receiver (Rx), and channel distance/characteristic, as well as the number of *a*RIS elements. In particular, the scenario under investigation is a non-line-of-sight (NLOS), single-user single-input single-output (SU-SISO) 5G communication system operating at millimeter-wave frequencies. Moreover, the performance trade-off among the *a*RIS's parameters is also explored.

In addition to outlining the quantitative specification analysis of the *a*RIS's active circuit, this work also reveals the qualitative insightful characteristics of an *a*RIS-assisted system as summarized below.

- The Tx-to-Rx communication performance mainly relies upon the number of element N and the total output power of the *a*RIS.
- The reverse Rx-to-Tx communication is mainly dependent upon the number of element N.
- Typically, the noise contribution from an *a*RIS is negligible as compared to the receiver's noise.
- The benefits of a higher N not only relaxes the gain and linearity requirement in *a*RIS's active circuit, but also results in less power consumption, albeit at the expense of higher implementation cost and complexity.

2. SIGNAL AND SYSTEM MODELS

2.1 SIGNAL MODEL OF *a*RIS

An active RIS (*a*RIS) is composed of an array of active reflectors, which in turn comprises a passive antenna, a programmable phase shifter and a variable-gain reflection-type amplifier [6], [11]. A typical signal model of an N-element *a*RIS shown in Fig. 1 is given by

$$\mathbf{y} = \mathbf{\Psi}\mathbf{x} + \mathbf{\Psi}\mathbf{v}, \tag{1}$$

where $\mathbf{\Psi} = \mathrm{diag}\left(p_1 e^{j\theta_1}, p_2 e^{j\theta_2}, \dots, p_N e^{j\theta_N}\right) \in \mathbb{C}^{N\times N}$ denotes the reflection coefficient matrix with p_j being the gain and $\theta_j$the phase shift in the i^{th} element, $\mathbf{x} \in \mathbb{C}^N$ represents the incident wave, and $\mathbf{y} \in \mathbb{C}^N$ is the reflected signal from the *a*RIS. $\mathbf{v} = [v_1, v_2, \dots, v_N]^T$ denotes the equivalent input noise vector of the *a*RIS, modelled as additive complex multi-variate white Guassian noise with zero mean and variance σ_v^2, $\mathbf{v} \sim \mathcal{CN}(\mathbf{0}_N, \sigma_{vj}^2 \mathbf{I}_N)$.

The phase shifts associated with $\mathbf{\Psi}$ in (1) can be adjusted or reconfigured to form a beam in the reflected wave, or in other words, to coherently add the reflected signal from each *a*RIS element at the receiver. While all the gains p_j's are typically set identical, it can also be adjusted to suppress the side-lobe of the reflected beam.

2.2 *a*RIS-ASSISTED SU-SISO SYSTEM MODEL

The performance gain enabled by incorporating the *a*RIS to form a NLOS communication link assuming a single-user single-input single-output (SU-SISO) system can be investigated via the following link model;

$$r = \mathbf{f}^{\boldsymbol{H}}\mathbf{\Psi}\mathbf{g}\, s + \mathbf{f}^{\boldsymbol{H}}\mathbf{\Psi}\mathbf{v}\,, \tag{2}$$

where $r \in \mathbb{C}$ denotes the signal received by the user, $\mathbf{g} = [g_1, g_2, \dots, g_N]^T$ and $\mathbf{f} = [f, f_2, \dots, f_N]^T$ represents the Tx-to-*a*RIS and *a*RIS-to-Rx channel vectors, and s is the total signal from the transmitter propagating directly to the *a*RIS. It is noted that, for the downlink case, the transmitter is the base station (BS) while the receiver is the user element (UE), and vice versa for the uplink case.

For the case that each of the element's gains p_j, $\forall j \in \{1, \dots, N\}$, is identical, we have $\mathbf{\Psi} = p\mathbf{\Theta}$ where $\mathbf{\Theta} = \mathrm{diag}\left(e^{j\theta_1}, e^{j\theta_2}, \dots, e^{j\theta_N}\right)$. Following this and under the assumption $N \to \infty$, it can be derived that the maximum SNR (γ_{max}) at the receiver can be accomplished under the conditions [6]:

$$\theta_j^{\mathrm{opt}} = \angle f_j - \angle g_j, \forall j \in \{1, \dots, N\} \tag{3a}$$

$$p^{\mathrm{opt}} = \sqrt{\frac{P_{aRIS}^{max}}{P_{Tx}^{max}\sum_{j=1}^{N}|g_j|^2 + N\sigma_v^2}} \tag{3b}$$

$$\gamma_{max} = \frac{\pi^2}{16} \cdot \frac{N\varrho_g^2\varrho_f^2 P_{Tx}^{max} P_{aRIS}^{max}}{\sigma_v^2\varrho_f^2 P_{aRIS}^{max} + \sigma^2\varrho_g^2 P_{Tx}^{max} + \sigma^2\sigma_v^2}, \tag{3c}$$

where $\varrho_g^2 = \mathrm{PL}_g \cdot G_{aRIS} \cdot \cos(\varphi_g)$ and $\varrho_f^2 = \mathrm{PL}_f \cdot G_f \cdot \cos(\varphi_f)$, with φ_g and φ_f being the incident/reflected angles with reference to the normal angle of the *a*RIS, $G_{aRIS} = 4\pi A_{eg}/\lambda^2$ and $G_f = 4\pi A_{ef}/\lambda^2$ being the antenna gains of the *a*RIS and Rx where λ is the signal wavelength. $A_{eg} = N_g(\lambda/2)^2$ and $A_{ef} = N_f(\lambda/2)^2$ are the aperture areas of the *a*RIS and Rx antenna, respectively. Also, the path loss can be expressed as $\mathrm{PL}_g = \lambda^2/4\pi d_g^{\alpha}$ and $\mathrm{PL}_f = \lambda^2/4\pi d_f^{\beta}$, where α and β denote the path loss exponents of the Tx-*a*RIS channel and the *a*RIS-Rx channel, respectively. Note that α and β typically range from 2 to 4. Also note that the factor $\pi^2/16$ arises from the statistically independent characteristics with the Rayleigh distribution between Tx-to-*a*RIS the *a*RIS-to-Rx paths [3].

2.3 OPERATIONAL INSIGHTS AND REMARKS

Some important operational insight and remarks related to the signal and system models of the *a*RIS-assisted system can be deduced from the SNR equation in (3c) as follows.

First, unlike its passive counterpart where SNR $\propto N^2$, the *a*RIS's output SNR is proportional to the number of N [6]. This is mainly due to the effect of the amplifier's noise in the *a*RIS. Specifically, while the incident wave upon the active surface is collected, amplified and beamed via the controlled phase shift into the desired direction, yielding a gain of pN^2, the noise is increased by a factor of pN. Such a proportional relationship $\propto N$ stems from the fact that noise is random and thus transparent to the phase shift. Thus, unlike the incident signal, the noise is not beamed directly to the receiver. Even though SNR $\propto N$ in the *a*RIS, its absolute SNR value is still higher than its passive version. This is attributed to the signal amplification associated with the *a*RIS, which can significantly increase the received signal strength. As a consequence, the impact of the receiver's noise is negligible.

Secondly, under a typical downlink condition where $P_{Tx}^{max}\varrho_g^2 \gg P_{aRIS}^{max}\varrho_f^2$, (3c) can be approximated as $SNR \approx NP_{aRIS}^{max}\pi^2\varrho_f^2/16\sigma^2$, implying that the Tx-to-Rx commu-nication mainly relies upon the number of element N and power P_{aRIS}^{max} of the *a*RIS. One the other hand, under a typical uplink condition where $P_{aRIS}^{max}\varrho_f^2 \gg P_{Rx}^{max}\varrho_g^2$, (3c) can be expressed as $SNR \approx NP_{Rx}^{max}\pi^2\varrho_g^2/16\sigma_v^2$. This indicates that the reverse Rx-to-Tx communication is mainly dependent upon N and σ_v^2 of the *a*RIS.

Another important observation is that the up/down link performance can be both enhanced by employing more number of elements N. An additional benefit as indictaed by (3b) is a reduction in the gain requirement in the *a*RIS by increasing N, yielding less demand on its hardware complexity and total power consumption. All the remarks summarized above serve as a useful guideline when designing the up/down link budget of an *a*RIS-assisted communication system.

3. *a*RIS-ASSISTED SYSTEM: A CASE STUDY

3.1 COMMUNICATION SYSTEM SETUP

In this work, we consider a specific case example of an *a*RIS-assisted NLOS SU-SISO 5G communication system between a 5G base station (BS) (as a Tx) and one single user element (UE) (as an Rx) operating at 28 GHz. It is assumed that the direct link is negligible because of a severe obstruction. For the BS-*a*RIS channel, a fixed free space path loss exponent for a direct link at β = 2.0 is assumed, whereas two different *a*RIS-UE path loss exponents β = 2.0 and 2.8 were investigated, representing communication channels with a normal-link condition and a weak-link condition (in a more dense environment), respectively. The uplink and downlink modems are of quadrature-amplitude-modulation 16-QAM and 256-QAM types, yielding the SNR requirement at 23 and 33 dB, respectively.

The Tx-*a*RIS distance is fixed at 50 m, whereas the *a*RIS-to-Rx set at 5 m. The transmitting EIRP of the BS is assumed at 55 dBm, with a raw output power at 1 W and a Tx antenna directivity at 25 dBi. A noise factor (*NF*) of the BS's receiver is assumed at $NF_{BS} = 1$ dB. For the portable UE, a typical output power at -20 dBm, a gain at 10 dBi and a noise factor at $NF_{ue} = 3$ dB are assumed. The inclination angles between the Tx-*a*RIS and *a*RIS-UE are set at $\varphi_g = \varphi_f = 45^o$ as a worse-case scenario.

For the *a*RIS, the number of elements is set at $N = 128$ and the dimension of each element at 6 mm x 6 mm for a 28-GHz operating frequency. Since the link budget is somewhat insensitive to the *a*RIS's noise factor, $NF_{aRIS} = 12$ can be tolerated. Note that, in our calculation, it is approximated for simplicity that the gain and directivity in each of the employed antennas are identical.

3.2 LINK BUDGET AND HARDWARE SPECIFICATION

Having set up all the parameters, we are now ready to determine the specification of the *a*RIS, including the *a*RIS's total output power P_{aRIS}^{max} and the optimum power gain G_{aRIS} in each of the active element, so as to meet the uplink/downlink SNR requirement under the specified communication system in Section 3.1. The *a*RIS's antenna element is assumed to be a 28-GHz microstrip patch type with a 4.46-dBi gain (including a 1.5-dB loss) and 6.0 mm × 6.0 mm dimensions.

With the use of (3) and the MATLAB software [11] for numerical computation, the plot of SNR_{UE} and G_{aRIS} versus P_{aRIS}^{max} at the normal *down*link condition β = 2.0 can be shown in Fig. 2(a). Based on the downlink SNR requirement of 33 dB with a 3-dB margin, the plots indicate the optimum gain and output power of the *a*RIS at G_{aRIS}^{opt} = 10.4 dB and P_{aRIS}^{max} = 0.65 mW. Also indicated in Fig. 2(a) is the plot of SNR_{BS} and G_{aRIS} versus P_{aRIS}^{max} at β = 2.0 the corresponding *uplink* condition. At the optimum gain G_{aRIS}^{opt} = 10.4 dB, the uplink SNR at 31 dB is obtained, meeting the 23-dB requirement with >8-dB margin.

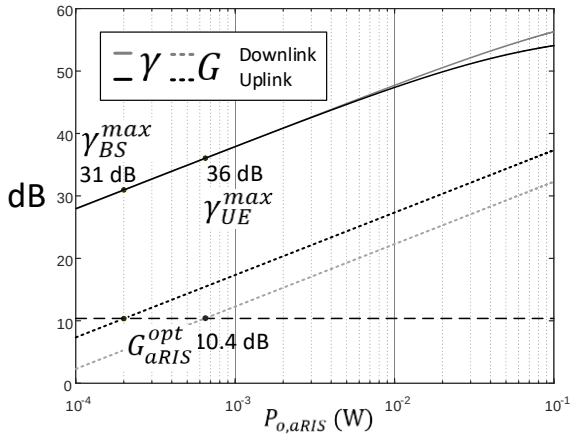

(a)

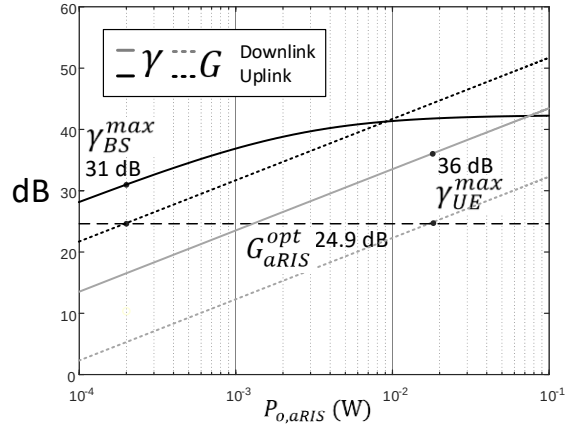

(b)

Fig. 2 *a*RIS performance requirement for (a) normal *a*RIS-to-UE link and (b) weak UE-to- *a*RIS link.

Before proceeding to the case of a weak-link condition, it is instructive to investigate the power levels along the up/down links via the conventional level diagram as illustrated in Fig. 3(a) and 3(b) (on the next page). As evident from the diagrams, at G_{aRIS}^{opt} = 10.5 dB, SNR_{ue} = 33 dB and SNR_{bs} = 37.9 dB are obtained. These values are higher than those in the plots of Fig. 3 based on (3c) by about 2.0 dB. This is primarily due to the factor $\pi^2/16$ in the equation (3c), which is attributed to the Rayleigh distribution between two statistically independent Tx-to-*a*RIS and *a*RIS-to-Rx paths in the formulation as mentioned in Section 2.2. Also notice that the amplification of the noise σ_v^2 associated with the *a*RIS is less than that of the incoming Tx signal by a factor of N = 128 (~10 dB), because its random amplitude and phase are transparent to the beamforming process by virtue of phase-shifting as explained in Section 2.3. Another important observation from both the up/down link's level diagrams is a negligible impact of the noise σ_v^2 associated with the *a*RIS as compared to the associated noise σ_l^2 of the corresponding receiver, because of a high free-space-loss attenuation of the *a*RIS-to-Rx path. However, with a continued increase of P_{aRIS}^{max}, and subsequently the *a*RIS gain (as the incoming signal power is constant), the impact of σ_v^2 will become higher and eventually comparable to σ_l^2 at the receiver, yielding a maximum achievable SNR at the receiver equal to the *a*RIS's output SNR, independent on the *a*RIS's output power.

Let us now turn to the weak-link condition, i.e., β = 2.8. Similarly, with the use of (3b) and (3c), the plot of SNR_{UE} and G_{aRIS} versus P_{aRIS}^{max} can be given in Fig. 2(b). Under such a condition, based on the downlink SNR requirement, the plot suggests higher optimum gain and output power requirement of the *a*RIS at G_{aRIS}^{opt} = 24.9 dB and P_{aRIS}^{max} = 1.8 mW, respectively. For the uplink case at the optimum gain G_{aRIS}^{opt} = 24.9 dB, the uplink SNR at 31 dB is obtained, meeting the 23-dB requirement with almost 8-dB margin. Also indicated in the plots of Fig. 2(b) is the flattening of the uplink SNR as P_{aRIS}^{max} and hence G_{aRIS}^{opt} continued to increase, yielding a higher impact from the *a*RIS's noise, σ_v^2, as discussed earlier. The effect is more evident than that of Fig. 2(a) since the required *a*RIS's output power and gain are much higher in such a weak-link condition.

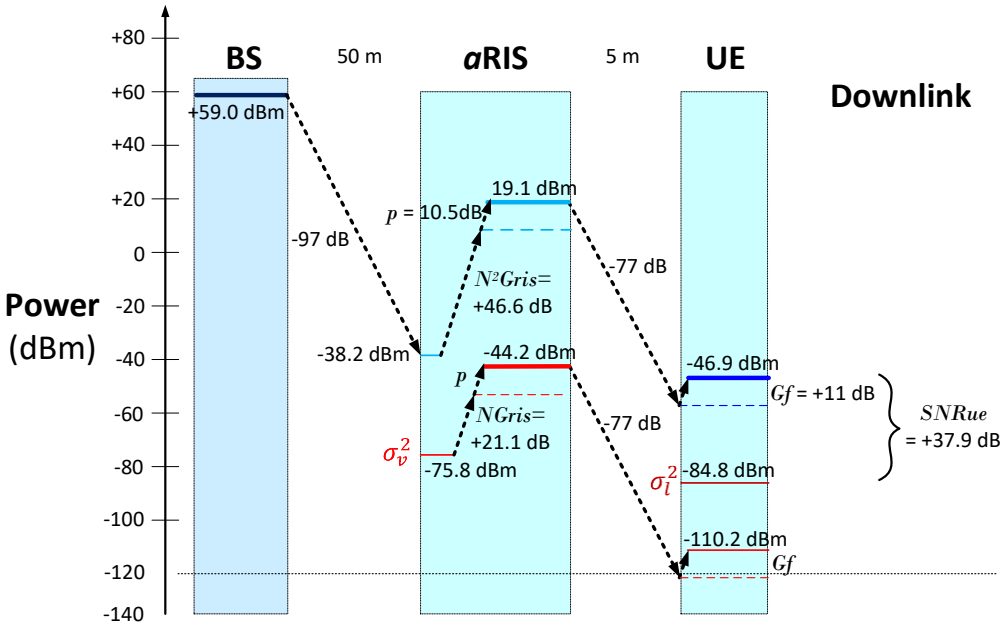

(a)

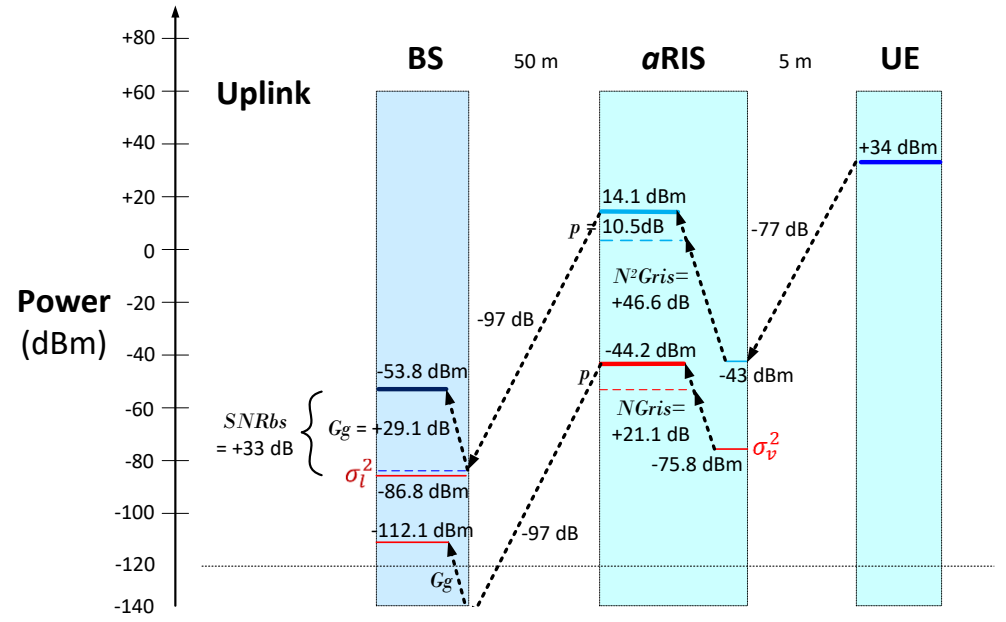

(b)

Fig. 3 *Level diagrams illustrating signal power at each point along the aRIS-assisted communication system (a) downlink case (b) uplink case, both at normal link condition.*

***Table 1**. aRIS Specifications at NF = 12 dB.*

Size/Electrical Parameters	N = 128 β = 2.0	N = 128 β = 2.8	N = 256 β = 2.8
Optimum Gain	10.4 dB	24.9 dB	18.7 dB
Output 1-dB Compression	-16.9 dBm	-12.5 dBm	-18.5 dBm
Total Power Consumption*	0.65 W	1.80 W	0.90 W

* Real value may vary significantly depending on practical implementation.

Based on the plots of Fig. 2 and 3, the resulting specification of the *a*RIS that meets the communication system performance under the assigned parameters and link conditions can be summarized in Table 1. It is noted that the output 1-dB compression point in *each* active element was calculated by a margin of 6-dB from the required P_{aRIS}^{max}, whereas the total dc power requirement was calculated from the equation P_{aRIS}^{max}/η by assuming an implementation efficiency η at 0.1%. Finally, the reflection's phase shift associated with each element are determined according to (3a). Note that, in practice, the resolution of the phase shifts in each element can be quantized to only 3 bits while still achieving a good performance [12].

Let us explore the design trade-off by doubling the number of elements to N = 256, and hence the size of the *a*RIS. Based upon (3b) and (3c), we obtain G_{aRIS}^{opt} = 18.7 dB and $P_{o,aRIS}$ = 0.9 mW in order to meet the communi-cation performance at the weak-link condition. These values are about half of those obtained at N = 128, indicating reduction in both the gain requirement and power consumption by enlarging the *a*RIS size, albeit at the expense of more hardware complexity. This performance trade-off may be useful in some practical implementation, particularly when an achievable gain and a total power consumption in the employed active circuit are major constraints.

4. CONCLUSION

This work has investigated a hardware requirement of an active reconfigurable intelligent surface by virtue of the link budget calculation of an *a*RIS-assisted NLOS communication system. Important characteristic and operation of the *a*RIS were discussed. Without loss of generality, a specific SU-SISO NLOS wireless system operating at 28 GHz was employed to determine the gain, power and linearity of the *a*RIS's active circuit, under both normal and weak path loss conditions. To serve as a design guideline, a discussion on performance trade-off was given, highlighting several benefits of enlarging the *a*RIS size. In particular, it has been shown that a higher number of elements not only yields a lower gain, lower linearity requirement, but also a power reduction in the active circuits, at the expense of higher implementation cost and complexity.

REFERENCES

[1] M. Di Renzo, et al., "Smart Radio Environments Empowered by Reconfigurable Intelligent Surfaces: How it works, state of research, and the road ahead," IEEE J. Sel. Areas Commun., vol. 38, no. 11, pp. 2450–2525, Nov. 2020.

[2] L. Zhang, et al., "Spacetime-Coding Digital Meta-surfaces," Nature Communication, vol. 9, no. 4338, Oct. 2018.

[3] Q. Wu and R. Zhang, "Intelligent Reflecting Surface Enhanced Wireless Network via Joint Active and Passive Beamforming," in IEEE Transactions on Wireless Communications, vol. 18, no. 11, pp. 5394-5409, Nov. 2019.

[4] R. Long, et al., "Active Reconfigurable Intelligent Surface-Aided Wireless Communications," in IEEE Transactions on Wireless Communications, vol. 20, no. 8, pp. 4962-4975, Aug. 2021.

[5] W. Tang et al., "Path Loss Modeling and Measurements for Reconfigurable Intelligent Surfaces in the Millimeter-Wave Frequency Band," in IEEE Transactions on Communications, vol. 70, no. 9, pp. 6259-6276, Sept. 2022.

[6] Z. Zhang et al., "Active RIS vs. Passive RIS: Which Will Prevail in 6G?," in IEEE Transactions on Communications, vol. 71, no. 3, pp. 1707-1725, March 2023.

[7] K. K. Hishor, and S. V. Hum, "An Amplifying Reconfigurable Reflectarray Antenna," in IEEE Transactions on Antennas and Propagation, vol. 60, no. 1, pp. 197-205, Jan. 2012.

[8] J. -B. Gros, V. Popov, M. A. Odit, V. Lenets and G. Lerosey, "A Reconfigurable Intelligent Surface at mmWave Based on a Binary Phase Tunable Metasurface," in IEEE Open Journal of the Communications Society, vol. 2, pp. 1055-1064, 2021.

[9] L. Dai *et al*., "Reconfigurable Intelligent Surface-Based Wireless Communications: Antenna Design, Prototyping, and Experimental Results," in *IEEE Access*, vol. 8, pp. 45913-45923, 2020.

[10] J. F. Bousquet, S. C. Magierowski and G. G. Messier, "An Integrated Active Reflector for Phase-Sweep Cooperative Diversity," in IEEE Transactions on Circuits and Systems II: Express Briefs, vol. 56, no. 8, pp. 624-628, Aug. 2009.

[11] The MathWorks, Inc. (2016). *MATLAB version: 9.0 (R2016b)*.

[12] A. Worapishet, "A Numerical Investigation of Gain and Phase Errors of Unit Elements on Performance of Active Reconfigurable Intelligent Surface", ENGINEERING TRANSACTIONS, vol. 26, no. 2 (55) July-Dec, 2023

Apisak Worapishet received the B.Eng. (First-class Hons.) degree from the King Mongkut's Institute of Technology Ladkrabang, Bangkok, Thailand, in 1990, the M.Eng.Sc. degree from the University of New South Wales, Kensington, NSW, Australia, in 1995, and the Ph.D. degree from the Imperial College London, London, U.K., in 2000, all in electrical engineering.

Since 1990, he has been with the Mahanakorn University of Technology, Bangkok, Thailand, where he is currently a Professor of electronic engineering. He has also served as a Visiting Professor in RF IC Design at the University College Doublin since 2023. His research interests include analogue integrated circuits, passive/active RF/microwave circuits, and wireless power

transfer.

Dr. Worapishet served as an Associate Editor for the IEEE TRANSACTIONS ON CIRCUITS AND SYS-TEMS I: REGULAR PAPERS for six years (from 2016 to 2022). He was also the Editor-in-Chief for ECTI Transactions on Electrical Engineering, Electronics, and Communications. He is an IEEE Senior member, a member of the Analog Signal Processing Technical Committee and the IEEE Circuits and Systems Society. He was the recipient of the British Council Researcher Exchange Program Award in 2009.